Vehicle suspension force and road profile prediction on undulating roads

Herman A. Hamersma* and P. Schalk Els
Department of Mechanical and Aeronautical Engineering, University of Pretoria, Pretoria, South Africa

*CONTACT Herman A. Hamersma. email: hermanh@up.ac.za

Abstract
Controllable suspension systems have the capability of changing suspension forces. One control approach is to define a cost function with the aim of optimising either ride comfort or handling. Such controllers are usually reactive and not pro-active. Controllers can benefit significantly by having a priori knowledge of the effect that changing the suspension settings will have on the suspension forces. This is especially true for vehicles traversing very rough terrain. This paper addresses the a priori knowledge needed by predicting what the suspension forces will be before changing the suspension setting. The proposed approach involves estimating sprung and unsprung mass acceleration, estimating the road excitation, and then predicting the suspension forces. A quarter car model is used to illustrate the concept. Thereafter, the concept is extended to a nonlinear multibody dynamics model and finally validated experimentally. Results indicate that the suspension force in a different suspension modes can be predicted before switching suspension modes.

Keywords: Suspension force prediction, road profile estimation, undulating roads, nonlinear suspension, suspension control

1. Introduction

The aim of the proposed estimator and predictor is to predict the effect a change in suspension settings will have on the vehicle's dynamic response before the change in suspension settings is made. The efficacy of advanced driver assist systems (ADAS) such as ABS, traction control, torque vectoring and others deteriorate significantly on undulating roads [1,2]. By changing or modulating the suspension settings, the performance of these systems may be improved. The control system thus needs to make a decision regarding spring and damper settings, and the proposed estimator and predictor is capable of giving information to the controller before it makes its control decision.

1.1. Background

The use of controllable suspensions is prevalent throughout the vehicle industry. Semi-active suspensions are used on a wide array of vehicles, from heavy vehicle applications, such as military, mining and agricultural vehicles to high performance passenger vehicles and Sports Utility Vehicles (SUVs). The advantage of using a controllable suspension on a

vehicle is that improved ride comfort and safety of a vehicle can be achieved compared to a passive suspension system [3,4]. Controllable suspension systems require a decision to be made regarding the switching of valves to achieve different spring or damper characteristics [5] or selecting a continuously variable setting between two limits (e.g. for the case of a magneto-rheological damper [6]). In the majority of these cases, *a priori* knowledge of the dynamic response of the vehicle after executing the control decision may improve the decision making significantly.

The aim of this study is to predict the suspension forces of a vehicle in suspension settings that differ from the current setting when driving over an undulating road. The predicted forces will be compared with the actual forces (modelled theoretically and measured experimentally) in the current suspension setting and with modelled forces in an alternate suspension setting. If this could be successfully achieved, the controller can evaluate vehicle performance (ride, handling, etc.) for all possible suspension settings simultaneously and select the best settings for the current optimal controller.

This paper is structured as follows: Section 1.2 discusses existing literature on the prediction of suspension forces based on the current vehicle state for different suspension settings. Section 2 introduces the suspension force prediction algorithm and illustrates its application to a linear quarter car model. Section 3 applies the algorithm to a fully nonlinear multibody dynamics model of a vehicle. Section 4 applies the algorithm to experimental results. Finally a conclusion is drawn and recommendations are made.

1.2. Existing approaches in the literature

Gillespie [7] states that all the primary control and disturbance forces that are applied to a vehicle, with the exception of the aerodynamic forces, are generated in the tyre-road contact patch. This is confirmed by Imine, Delanne [8] where the basic control inputs, sources of excitation and the resulting dynamic response is illustrated schematically.

Knowledge of the road profile is thus extremely important for the vehicle designer. A detailed description of the measurement techniques employed to determine the road profile is discussed by Becker and Els [9]. These methods include the use of single-wheel trailers [8], inertial profilometers [10], laser scanners [9] and high resolution cameras [11] that give geometrically accurate 3D models of the terrain. The limitation of these techniques is that they are time consuming and require significant amounts of post-processing, thus limiting their application to online control strategies.

The reporting of road profiles is covered in depth by ISO 8608:2016. The ISO 8608:2016 standard specifies that road profiles are reported as either displacement power spectral densities (PSDs) or acceleration PSDs. PSDs are reported versus spatial frequency (cycles/m or rad/m) [12]. Agostinacchio, Ciampa [13] illustrated a method of reconstructing road profiles from ISO 8608:2016.

Several publications focusing on road profile estimation was published by collaborating research groups at the Université de Versailles and the Laboratoire Centreal de Ponts et Chaussées in France [8,14,15]. Their work established several methods of estimating the road profile online, including adaptive observers [14] and several sliding mode observer strategies [8,15]. The estimation results were compared with road profiles measured with a longitudinal profile analyser – a single-wheel trailer that is towed behind a car at a constant speed. The trailer is an inertial pendulum and makes use of inertial measurements and

relative displacements to indirectly measure the road profile. The estimation results were used to estimate the tyre vertical forces under each wheel on a four-poster rig. The tyre vertical force estimation results are compared with force measurements of the four-poster rig's actuators [16].

Doumiati, Victorino [17] used a linear Kalman filter to estimate the road profile. The measurement inputs to the Kalman filter consisted of the suspension deflections, vehicle body vertical displacement (obtained by double integrating vertical acceleration) and the filtered vertical acceleration of the vehicle body. Doumiati, Martinez [18] improved on the Kalman filter strategy used by Doumiati, Victorino [17] by implementing Q-parameterisation. Two main advantages were obtained by using Q-parameterisation rather than Kalman filtering, namely that the Q-parameterisation is a less costly method requiring fewer observations and that it has a simpler tuning approach.

Ben Hassen, Miladi [19] estimated the road profile through the implementation of a new, fast and simple technique known as Independent Component Analysis. Four models were studied, namely a quarter car, a half car (pitch-bounce and a roll model) and a full car model. The advantage of using this method is the limited and easily obtainable observations needed: sprung mass vertical acceleration and the suspension deflection. No experimental validation of the results was included in this study.

Very little literature is available on suspension force prediction where the predicted force is for a change in suspension parameter or characteristics. There are numerous examples where the vehicle states such as heave, pitch, roll and the unsprung mass vertical motions are estimated making use of numerous estimation techniques. The interested reader is referred to Ray [20], Antonov, Fehn [21], Pence, Fathy [22] and Wenzel, Burnham [23] for some examples. Vazquez, Vaseur [24] developed a road profile and suspension state estimator with a Kalman filter technique. The technique was validated with a high fidelity simulator on sinusoidal road profiles at various speeds. Furthermore, experimental validation was done to validate the state estimation portion of the observer they developed with excellent robustness.

1.3. Research question

The aim of this study, however, is to predict the suspension force with a change in the force-displacement and force-velocity characteristics. If the suspension system was able to switch from one state to another instantaneously, the force at that precise moment in time can be calculated from the suspension displacements and velocities, but the vehicle response at any other point in time will be unknown. Many control strategies that aim to adapt the suspension system from one setting to another rely on an average value (i.e. historical values), such as the running root mean square (RMS) of vertical acceleration [3], to make their control decision. Knowledge of the vehicle's dynamic response at a single point in time is thus not good enough to justify switching the suspension from one setting to another. Knowledge of the relevant vehicle states and of the suspension force-displacement and force-velocity characteristics enables one to calculate the suspension forces in the current suspension mode, but not if the suspension mode was to be switched to a different mode, especially if a statistics-based metric such as RMS or standard deviation is used to inform such a control decision. This is gap in the literature is what this paper hopes to address.

2. Linear quarter car implementation

The proposed approach used to predict the suspension forces in this paper is by using two linear Kalman Filters (KF) [25] and a suitable vehicle dynamics predictor model. The approach is first detailed using a quarter car model, then it is extended to a fully nonlinear multi-body dynamics vehicle model (Section 3) and finally validated experimentally in Section 4. The prediction algorithm consists of the following steps:

(1) Estimate the sprung mass and unsprung mass vertical kinematics with a linear KF.
(2) Use the estimated results of Step 1 in a KF to estimate the road excitation.
(3) The estimated road excitation is given as input to a second linear quarter car model. The second linear quarter car model (the predictor model) uses the changed suspension settings and predicts the suspension forces based on the estimated road excitation.

The fundamental assumption being made is that the road profile that lies ahead does not deviate significantly from that which has already been traversed. This approach will thus have limited benefits when traversing a single discrete obstacle such as a speed bump.

The measurements needed for the suspension force predictor algorithm consist of:

(1) Relative suspension displacement
(2) Unsprung mass vertical acceleration
(3) Sprung mass vertical acceleration
(4) Sprung mass pitch and roll rates when the observer model is extended beyond a linear quarter car model (see Sections 3 and 4)

The measurements needed are thus relatively simple and may be performed with cost-effective sensors that can easily be integrated to any ground vehicle. The linear quarter car model used to introduce the predictor algorithm, as well as the road profile, is shown in Figure 1. The equations of motion pertaining to the linear quarter car are given in Equations (1) and (2). The model parameters are presented in Table 1.

$$M\ddot{z}_2 = k(z_1 - z_2) + c(\dot{z}_1 - \dot{z}_2) \tag{1}$$

$$m\ddot{z}_1 = k(z_2 - z_1) + c(\dot{z}_2 - \dot{z}_1) + k_t(z_0 - z_1) + c_t(\dot{z}_0 - \dot{z}_1) \tag{2}$$

The quarter car model is excited by the input road profile. A random ISO 8608:2016 Class D road profile was generated in the spatial domain with a maximum spatial frequency of 25 cycles/m up to 0.04 cycles/m [12]. The quarter car model was driven over the Class D road profile at a constant speed of 60 km/h. ISO 8608:2016 describes the road profile as a PSD of the vertical displacement of the form given in Equation (3) [12]. The constants used for the road profile generation were $n_0 = 0.1$cycles/m and $G_d(n_0) = 1024 \times 10^{-6}\text{m}^3$ with a fit exponent of $w = -2$. The randomly generated road profile is also shown in Figure 1. The Fourier transform magnitude is determined from the displacement PSD with Equation (4). Random phase information is then generated and the Fourier transform of the road profile is then described by Equation (5). An inverse Fourier transform of $F(i\omega)$ yields the road

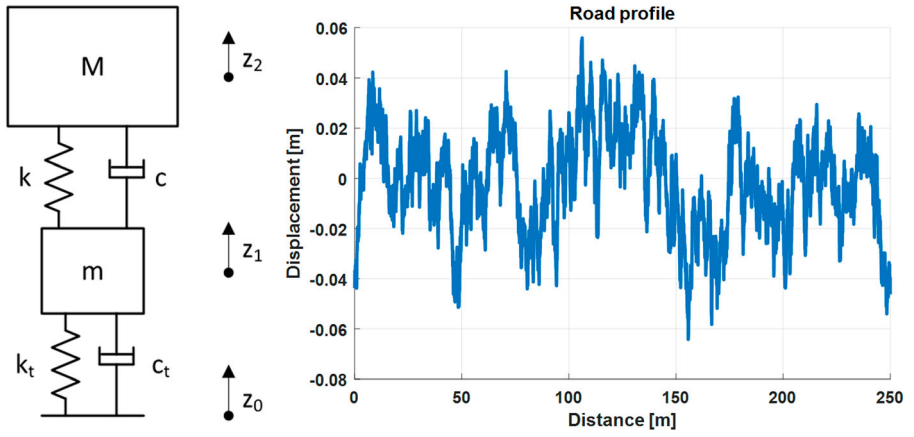

Figure 1. Linear quarter car model and road profile.

Table 1. Quarter car model parameters.

Parameter	Value	Unit
M	450	[kg]
m	80	[kg]
k	15e3	[N/m]
k_t	450e3	[N/m]
c	1000	[N.s/m]
c_t	10	[N.s/m]
$f_{n,usm}$	12.13	[Hz]
$f_{n,sm}$	0.90	[Hz]

profile in the spatial domain.

$$G_d(n) = G_d(n_0) \cdot (n/n_0)^{-w} \tag{3}$$

$$|F(i\omega)| = \sqrt{G_d(n) \cdot {}^{f_n}/_{n_{PSD}}} \tag{4}$$

$$F(i\omega) = |F(i\omega)| \cos\alpha + i|F(i\omega)| \sin\alpha \tag{5}$$

The linear quarter car model was modelled using Matlab Simulink [26]. A fourth order Runge–Kutta solver with a fixed time step of 1 ms was used to solve the differential equations describing the system.

2.1. The Kalman filter

Kalman Filtering is also known as linear quadratic estimation. The estimation technique makes use of two steps, a prediction step and a correction step. The prediction step requires an observer model that uses states estimated in the previous time steps to predict the states at the current time step. The correction step updates these estimates based on noisy observations from sensors. The proposed estimator makes use of a simple kinematic observer model of the vehicle and easy to measure states as observations.

The KF assumes that the states of the next time step develop from the states at the current time step, where $\boldsymbol{x}_k$ is the state vector at time step k, $\boldsymbol{F}$ is the state transition matrix, $\boldsymbol{B}$ is the

control matrix, $\boldsymbol{u_k}$ is the control vector and $\boldsymbol{w_k}$ is the process noise (see Equation (6)). The process noise has covariance $\boldsymbol{Q_k}$ at time step k. An observation of some of the states in $\boldsymbol{x}_k$ is made, according to Equation (7), where $\boldsymbol{z}_k$ is the observation vector, $\boldsymbol{H}$ is the observation model, and $\boldsymbol{v}_k$ is the observation noise. The observation noise has covariance $\boldsymbol{R}_k$ at time step k. The subscript $k|k-1$ indicates that the *a priori* information up to, but not including, time step k is used and this is found in the prediction step of the algorithm. The subscript $k|k$ is the corrected estimate using information up to and including time step k [25].

$$\boldsymbol{x}_k = \boldsymbol{F}\boldsymbol{x}_{k-1} + \boldsymbol{B}\boldsymbol{u}_k + \boldsymbol{w}_k \tag{6}$$

$$\boldsymbol{z}_k = \boldsymbol{H}\boldsymbol{x}_k + \boldsymbol{v}_k \tag{7}$$

The first step is the prediction step, predicting the state estimate and its covariance:

$$\hat{\boldsymbol{x}}_{k|k-1} = \boldsymbol{F}\hat{\boldsymbol{x}}_{k-1|k-1} + \boldsymbol{B}\boldsymbol{u}_k \tag{8}$$

$$\boldsymbol{P}_{k|k-1} = \boldsymbol{F}\boldsymbol{P}_{k-1|k-1}\boldsymbol{F}^T + \boldsymbol{Q}_{k-1} \tag{9}$$

The second step is updating the measurement residual $\tilde{\boldsymbol{z}}_{\boldsymbol{k}}$ and its covariance $\boldsymbol{S_k}$:

$$\tilde{\boldsymbol{z}}_{\boldsymbol{k}} = \boldsymbol{z}_k - \boldsymbol{H}\hat{\boldsymbol{x}}_{k|k-1} \tag{10}$$

$$\boldsymbol{S}_k = \boldsymbol{H}\boldsymbol{P}_{k|k-1}\boldsymbol{H}^T + \boldsymbol{R}_k \tag{11}$$

The optimal Kalman gain is then calculated:

$$\boldsymbol{K}_k = \boldsymbol{P}_{k|k-1}\boldsymbol{H}^T\boldsymbol{S}_k^{-1} \tag{12}$$

Finally, the state estimate and its covariance are updated:

$$\hat{\boldsymbol{x}}_{k|k} = \hat{\boldsymbol{x}}_{k|k-1} + \boldsymbol{K}_k\tilde{\boldsymbol{z}}_k \tag{13}$$

$$\boldsymbol{P}_{k|k} = (\boldsymbol{I} - \boldsymbol{K}_k\boldsymbol{H})\boldsymbol{P}_{k|k-1} \tag{14}$$

One limitation of the KF is that it applies only to linear systems, because it relies on the transition matrix $\boldsymbol{F}$ to develop the new states from the old states. Several extensions of the KF have been published, most notably the Extended KF and the Unscented KF. However, for the purposes of this study, a simple linear KF with time invariant $\boldsymbol{Q}$ and $\boldsymbol{R}$ matrices sufficed, rendering the subscript k in Equations (9) and (11) redundant. There is potential for further improving the approach by dynamically updating the noise characteristics, but this falls outside of the scope of this paper.

2.2. Step 1: Estimating the sprung mass and unsprung mass displacement

The first KF is used to estimate the sprung mass and unsprung mass displacement. The observer model used for this estimator is purely kinematic and relies on measuring the sprung mass and unsprung mass vertical acceleration and the relative suspension displacement and disregards the suspension force (stiffness and damping characteristics). To remove some of the integration drift, the sprung mass vertical displacement is given as a high uncertainty measurement of zero. This forces the sprung mass to oscillate about the zero position. The high uncertainty is indicated in the measurement covariance matrix,

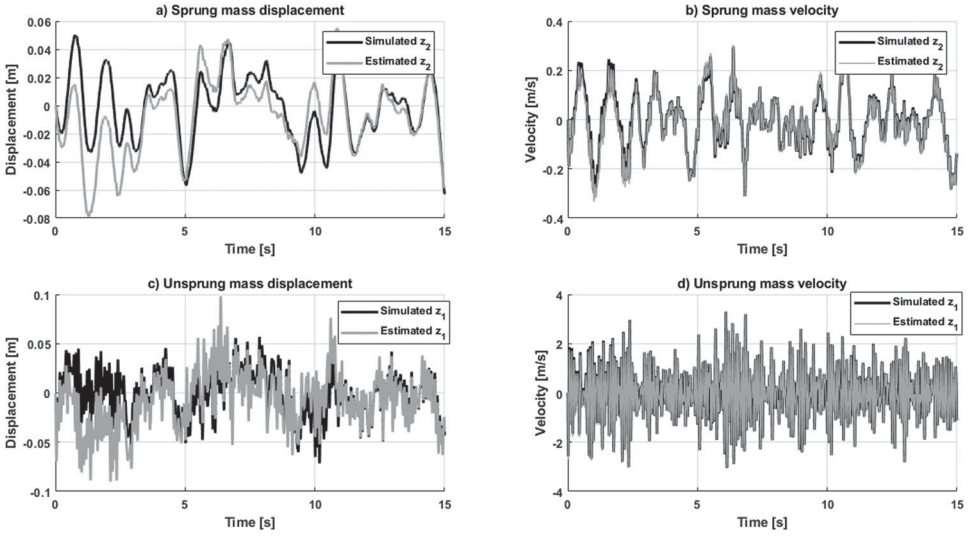

Figure 2. Sprung and unsprung mass displacement estimation results.

assigning it a value of 1e6 where the suspension strut displacement is assigned a value of one. The sprung and unsprung mass displacement observer model is given in Equation (15) and the measurement vector in Equation (16). Figure 2 shows the sprung and unsprung mass displacement simulation and estimation results using the road input of Equation (3). The estimation results show that the velocities are matched very accurately for both the sprung and unsprung masses. The displacement results show some slight discrepancies. This may be caused by the high uncertainty 'measurement' of the sprung mass displacement. Removing the high uncertainty measurement will however render the model unobservable and is thus required.

$$\begin{Bmatrix} z_1 \\ \dot{z}_1 \\ z_2 \\ \dot{z}_2 \end{Bmatrix}_k = \begin{bmatrix} 1 & \Delta t & 0 & 0 \\ 0 & 1 & 0 & 0 \\ 0 & 0 & 1 & \Delta t \\ 0 & 0 & 0 & 2 \end{bmatrix} \begin{Bmatrix} z_1 \\ \dot{z}_1 \\ z_2 \\ \dot{z}_2 \end{Bmatrix}_{k-1} + \begin{bmatrix} 0.5\Delta t^2 & 0 \\ \Delta t & 0 \\ 0 & 0.5\Delta t^2 \\ 0 & \Delta t \end{bmatrix} \begin{Bmatrix} \ddot{z}_1 \\ \ddot{z}_2 \end{Bmatrix}_k \tag{15}$$

$$\boldsymbol{z_k} = \begin{bmatrix} -1 & 0 & 1 & 0 \\ 0 & 0 & 1 & 0 \end{bmatrix} \begin{Bmatrix} z_1 \\ \dot{z}_1 \\ z_2 \\ \dot{z}_2 \end{Bmatrix}_k \tag{16}$$

2.3. Step 2: Estimating the road excitation

The second step of the suspension force prediction algorithm is to estimate the road excitation. This is also done with a linear Kalman Filter, but the road excitation estimation requires an observer model that includes kinetics. The following parameters need to be known:

(1) Current suspension setting force characteristics (spring stiffness and damping coefficient in the case of the linear quarter car)
(2) Tyre vertical stiffness

Although tyre vertical damping was included in Equation (2), this is often very difficult to determine. The tyre vertical damping is known to be very low, especially in cases of tyres with large aspect ratios as used on off-road vehicles [27]. For the road profile estimation, the tyre vertical damping was thus neglected. It will be demonstrated in this section that the road profile estimation still gives acceptable results with this assumption. Referring to the quarter car model of Figure 1, the observer model and measurement vector are given in Equations (17) and (18), respectively. The sprung and unsprung mass displacement estimation results are used as control input and measurement observations. The 'hat' in the notation indicates estimated values, rather than directly measured values. The road profile is included as a state in the state vector and the corresponding process covariance is increased several orders of magnitude to allow for some uncertainty of its value.

$$\begin{Bmatrix} z_1 \\ \dot{z}_1 \\ z_0 \end{Bmatrix}_k = \begin{bmatrix} 1 & \Delta t & 0 \\ -\frac{\Delta t}{m}(k+k_t) & 1-\frac{\Delta t}{m}c & \frac{\Delta t}{m}k_t \\ 0 & 0 & 1 \end{bmatrix} \begin{Bmatrix} z_1 \\ \dot{z}_1 \\ z_0 \end{Bmatrix}_{k-1} + \begin{bmatrix} 0 & 0 \\ \frac{\Delta t}{m}k & \frac{\Delta t}{m}c \\ 0 & 0 \end{bmatrix} \begin{Bmatrix} \hat{z}_2 \\ \dot{\hat{z}}_2 \end{Bmatrix}_k \quad (17)$$

$$\boldsymbol{z_k} = \begin{bmatrix} 1 & 0 & 0 \\ 0 & 1 & 0 \end{bmatrix} \begin{Bmatrix} z_1 \\ \dot{z}_1 \\ z_0 \end{Bmatrix}_k \approx \begin{Bmatrix} \hat{z}_1 \\ \dot{\hat{z}}_1 \end{Bmatrix} \quad (18)$$

Figure 3 shows the actual road profile and the estimated road profile (Figure 3a). Also shown is a single-sided spectrum magnitude of the Fast Fourier Transform (FFT) of the actual and estimated road profile at the frequency range of interest (Figure 3c and d) along with a displacement power spectral density (Figure 3b). It is evident in Figure 3 that the estimation results accurately represent the road profile. There are some slight discrepancies at very low frequencies. This may be due to the high uncertainty measurement imposed on the sprung mass displacement in Step 1 (Section 2.2) and due to the fact that tyre damping is neglected. Figure 3b, c and d indicate that the estimation results are remarkably similar at the range of excitation frequencies present in the road profile.

It is important to note that the road profile is thus estimated and may also be used by suspension controllers to classify the type of road in conjunction with standards such as ISO 8608:2016 [12]. This may allow a controller to classify road roughness online and adapt the suspension, tyre pressure or braking algorithm accordingly.

2.4. Step 3: Predicting the suspension force

The final step in the suspension force prediction algorithm is using the estimated road profile as input to a quarter car model. The quarter car model used in this step is the same as that shown in Figure 1 and given in Equations (1) and (2), with the exception that the road input is now that estimated in Section 2.3 rather than that of Equation (3). For the prediction step, the tyre damping is neglected again, as the tyre damping is usually unknown and difficult to determine. The resulting suspension force prediction (including the static suspension force) is shown in Figure 4.

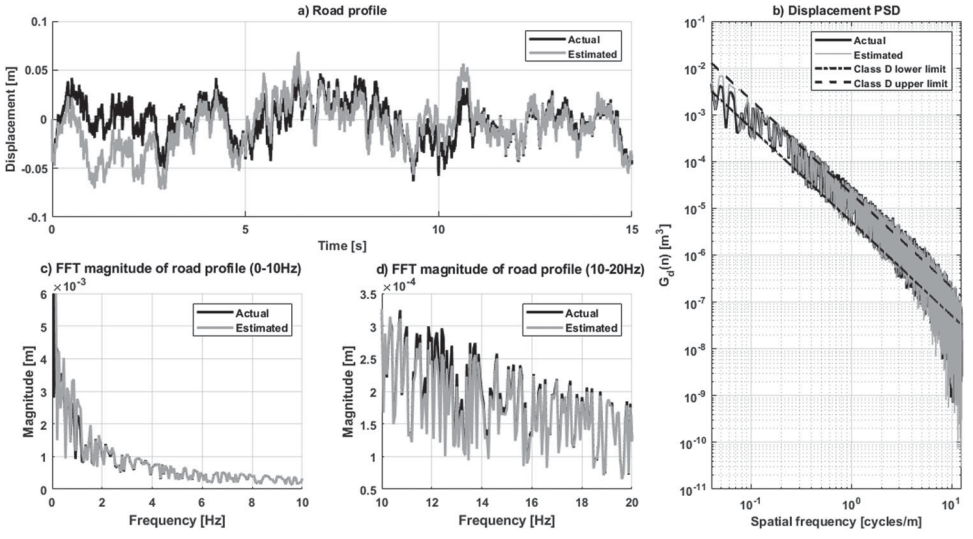

Figure 3. Road profile estimation results.

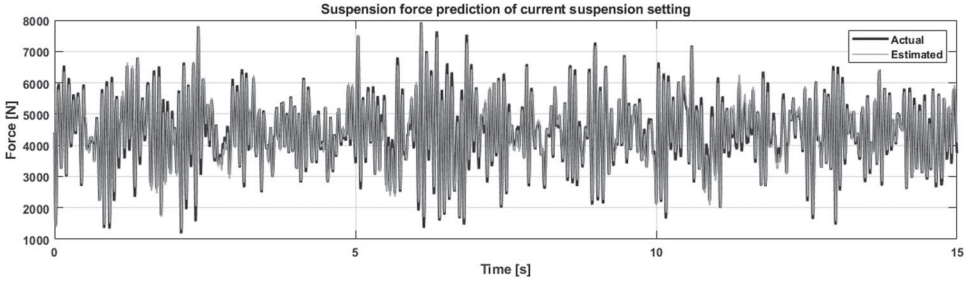

Figure 4. Suspension force prediction results at current suspension setting.

The prediction result shown in Figure 4 indicates that the suspension force prediction algorithm can accurately predict the suspension strut force when the suspension settings are left unaltered. The aim of the prediction algorithm, however, is to predict what the suspension settings will be if they are changed (without changing them). To investigate the prediction algorithm's capability, the quarter car model parameters are changed to new values. The suspension stiffness and damping values were changed to $k = 100$kN/m and $c = 4000$N.s/m. The modified suspension parameters are used together with the predictor model of Step 3. Additionally, a separate simulation is run with the modified parameters. The actual modelled suspension forces are compared with the predicted forces in Figure 5. It must be emphasised that the two results shown in Figure 5 share no information, it is based on two completely separate simulations, and only the inputs (road excitation) are the same. The prediction results in Figure 5 show an excellent correlation between the predicted and simulated suspension forces. The next step in evaluating the performance of the suspension force prediction algorithm is applying it to a fully nonlinear multibody dynamics model of a vehicle.

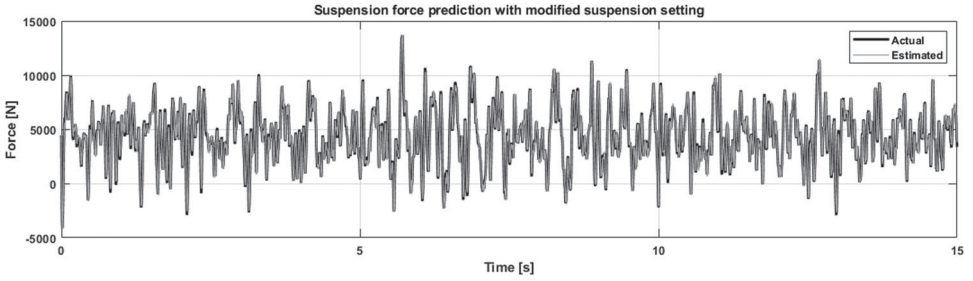

Figure 5. Suspension force prediction results with modified suspension setting.

Note that the tyre damping is excluded in the estimation and prediction models, but is indeed included in the simulation model that is excited by the road profile. This is how the suspension force prediction algorithm would be implemented in real life, with the real tyre having some damping and the estimator and predictor assuming that its contribution is negligible.

2.5. Analysis and discussion of results

The results of the linear quarter car implementation are very promising. Kat and Els [28] proposed a relative error metric to quantify the quality of estimated results. The validation metric gives a probability that the estimated value is below the mean relative error, with the mean relative error expressed as a percentage. This effectively indicates the probability that the relative error of the estimation is below the mean relative error. The following observations are made on the presented results:

(1) The mean relative error for the unmodified suspension force prediction is 3.76% with a 62.08% probability that the relative error is below the mean relative error. The relative error is below 10% for 94.38% of the time.
(2) The mean relative error of the modified suspension force prediction is 9.25% and the relative error is below the mean relative error 76% of the time.
(3) The road profile estimation successfully estimated the road profile to be a Class D road, as indicated in Figure 3b. The displacement spectral density indicates that the road profile is generally within the bounds of a Class D road as specified by ISO 8608:2016.

3. Full vehicle model implementation

The proposed algorithm, that gave excellent results in the linear quarter car implementation, is now expanded for a full vehicle model. Figure 6 provides an overview of the approach used in this section.

The observer and predictor models now employ a seven DOF linear vehicle model. To quantify the performance of this approach, estimation and prediction results are compared to simulations performed on a fully nonlinear multibody dynamics vehicle model. The fully nonlinear multibody dynamics vehicle model is based on a Land Rover Defender modelled in Adams [29] by Thoresson, Uys [30]. The process to determine the mass moments of inertia of the vehicle was described in detail by Uys, Els [31]. The vehicle

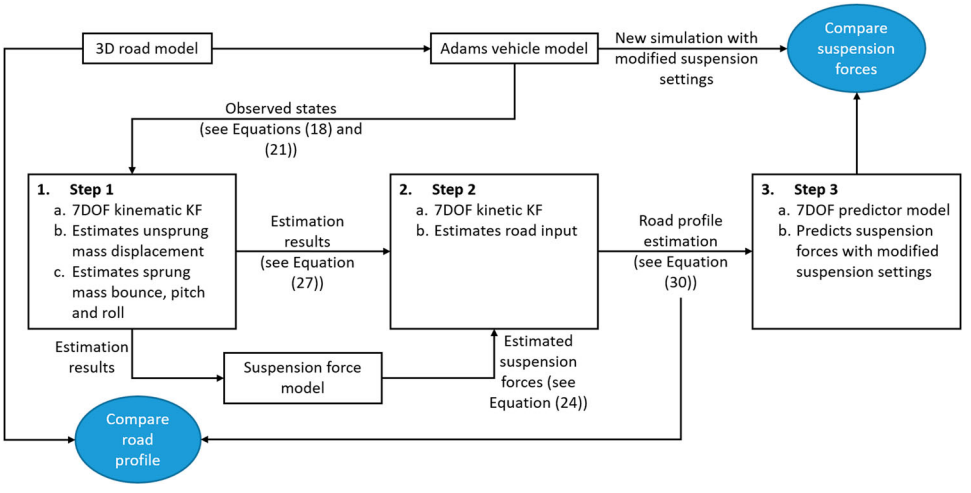

Figure 6. Simulation approach used in Section 3.

has leading arms and a Parnhard rod connecting to the front solid axle, trailing arms and an A-arm connecting to the rear axle, and an anti-roll bar fitted to the rear suspension. The simulation model contains sixteen (16) DOFs. The Land Rover Defender is also the experimental vehicle used in Section 4.

The vehicle's original passive suspension system was replaced by Els [3] with a hydropneumatic suspension that includes two gas accumulators and a valve manifold. The hydropneumatic suspension, called the Four State Semi-Active Suspension System ($4S_4$), allows the selection of two discrete force-displacement characteristics and two damping settings. The gas accumulators were modelled by Van der Westhuizen and Els [32] and the damping characteristics determined experimentally by Theron and Els [33]. The suspension model assumes adiabatic compression of the accumulator gas and heat transfer is accounted for by including the first law of thermodynamics (also known as the energy equation). The vehicle model includes the suspension kinematics, bump stops, suspension bushings and an FTire [34] tyre model, parameterised by Bosch, Hamersma [35]. The vehicle is simulated on experimentally measured road profiles [9] that were implemented as 3D regular grid roads (RGR). The experimental vehicle is driven over the exact same road profile in Section 4. This model has been developed over many years and has been extensively verified against experimental data for various suspension settings.

Els [3] developed a suspension control system that chose between two suspension modes, 'Ride Comfort' and 'Handling'. The 'Ride Comfort' mode utilises both accumulators and the lowest damping setting, resulting in a soft suspension that reduces the RMS of the sprung mass vertical acceleration. The 'Handling' suspension mode allows only the smaller of the two gas accumulators to be compressed and utilises the highest damping setting. The 'Handling' mode thus results in a stiffer suspension that prevents excessive body roll and the vehicle will start sliding before it rolls.

Since the model being used to perform the measurements for input to the algorithm is more complicated than the quarter car model of Section 2, the observer and predictor models used in Section 2 need to be modified to include more degrees of freedom. A seven

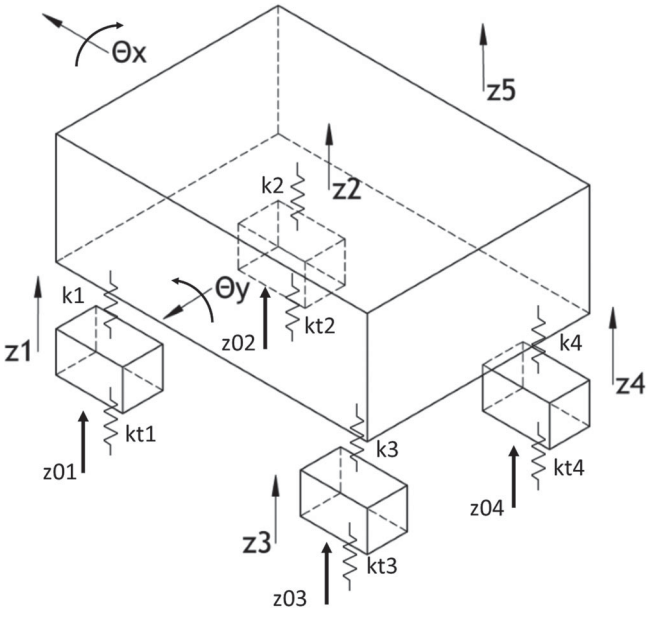

Figure 7. Seven degrees of freedom observer model (dampers not shown).

degree-of-freedom (DOF) model is used for the two observer models of Steps 1 and 2 and for the predictor model of Step 3.

3.1. Modified observer and predictor models

The modified observer and predictor models use a seven DOF approach. The seven DOF model is shown in Figure 7. Figure 7 does not show the suspension dampers and tyre damping effects, as this would clutter the image. The suspension damping effects are included in the equations of motion describing the model's response.

The kinematic observer model used for Step 1 of the suspension force prediction algorithm is given in Equations (19) to (24). The seven degrees of freedom in the modified model are the four unsprung mass vertical displacements, the sprung mass vertical displacement and roll and pitch motions. Since the observer model now contains more degrees of freedom (compared to the linear quarter car model implementation), additional control inputs and measurements are added. For the observer model of Step 1, the control vector (Equation (19)) consists of the vertical accelerations of the five masses in the model. The measurement vector (Equation (23)) consists of the four suspension strut displacements, the roll and pitch rates of the sprung mass and finally a high uncertainty measurement of the sprung mass vertical displacement.

Where

$$\boldsymbol{x}_k = \left\langle \; z_1 \quad \dot{z}_1 \quad z_2 \quad \dot{z}_2 \quad z_3 \quad \dot{z}_3 \quad z_4 \quad \dot{z}_4 \quad z_5 \quad \dot{z}_5 \quad \theta_x \quad \dot{\theta}_x \quad \theta_y \quad \dot{\theta}_y \; \right\rangle^T \tag{19}$$

And

$$\boldsymbol{u}_k = \left\langle \; \ddot{z}_1 \quad \ddot{z}_2 \quad \ddot{z}_3 \quad \ddot{z}_4 \quad \ddot{z}_5 \; \right\rangle^T \tag{20}$$

And

$$\boldsymbol{F} = \begin{bmatrix} 1 & \Delta t & 0 & 0 & 0 & 0 & 0 & 0 & 0 & 0 & 0 & 0 & 0 & 0 \\ 0 & 1 & 0 & 0 & 0 & 0 & 0 & 0 & 0 & 0 & 0 & 0 & 0 & 0 \\ 0 & 0 & 1 & \Delta t & 0 & 0 & 0 & 0 & 0 & 0 & 0 & 0 & 0 & 0 \\ 0 & 0 & 0 & 1 & 0 & 0 & 0 & 0 & 0 & 0 & 0 & 0 & 0 & 0 \\ 0 & 0 & 0 & 0 & 1 & \Delta t & 0 & 0 & 0 & 0 & 0 & 0 & 0 & 0 \\ 0 & 0 & 0 & 0 & 0 & 1 & 0 & 0 & 0 & 0 & 0 & 0 & 0 & 0 \\ 0 & 0 & 0 & 0 & 0 & 0 & 1 & \Delta t & 0 & 0 & 0 & 0 & 0 & 0 \\ 0 & 0 & 0 & 0 & 0 & 0 & 0 & 1 & 0 & 0 & 0 & 0 & 0 & 0 \\ 0 & 0 & 0 & 0 & 0 & 0 & 0 & 0 & 1 & \Delta t & 0 & 0 & 0 & 0 \\ 0 & 0 & 0 & 0 & 0 & 0 & 0 & 0 & 0 & 1 & 0 & 0 & 0 & 0 \\ 0 & 0 & 0 & 0 & 0 & 0 & 0 & 0 & 0 & 0 & 1 & \Delta t & 0 & 0 \\ 0 & 0 & 0 & 0 & 0 & 0 & 0 & 0 & 0 & 0 & 0 & 1 & 0 & 0 \\ 0 & 0 & 0 & 0 & 0 & 0 & 0 & 0 & 0 & 0 & 0 & 0 & 1 & \Delta t \\ 0 & 0 & 0 & 0 & 0 & 0 & 0 & 0 & 0 & 0 & 0 & 0 & 0 & 1 \end{bmatrix} \tag{21}$$

And

$$\boldsymbol{B} = \begin{bmatrix} & 0.5\Delta t^2 & 0 & 0 & 0 & 0 \\ & \Delta t & 0 & 0 & 0 & 0 \\ & 0 & 0.5\Delta t^2 & 0 & 0 & 0 \\ & 0 & \Delta t & 0 & 0 & 0 \\ & 0 & 0 & 0.5\Delta t^2 & 0 & 0 \\ & 0 & 0 & \Delta t & 0 & 0 \\ \Delta & 0 & 0 & 0 & 0.5\Delta t^2 & 0 \\ & 0 & 0 & 0 & \Delta t & 0 \\ & 0 & 0 & 0 & 0 & 0.5\Delta t^2 \\ & 0 & 0 & 0 & 0 & \Delta t \\ & 0 & 0 & 0 & 0 & 0 \\ & 0 & 0 & 0 & 0 & 0 \\ & 0 & 0 & 0 & 0 & 0 \\ & 0 & 0 & 0 & 0 & 0 \end{bmatrix} \tag{22}$$

Where

$$\boldsymbol{z}_k = \begin{pmatrix} x_{FL} & x_{FR} & x_{RL} & x_{RR} & \dot{\theta}_x & \dot{\theta}_y & z_5 \end{pmatrix}^T \tag{23}$$

And

$$\boldsymbol{H} = \begin{bmatrix} -1 & 0 & 0 & 0 & 0 & 0 & 0 & 0 & 1 & 0 & t_l & 0 & -l_f & 0 \\ 0 & 0 & -1 & 0 & 0 & 0 & 0 & 0 & 1 & 0 & -t_r & 0 & -l_f & 0 \\ 0 & 0 & 0 & 0 & -1 & 0 & 0 & 0 & 1 & 0 & t_l & 0 & l_r & 0 \\ 0 & 0 & 0 & 0 & 0 & 0 & -1 & 0 & 1 & 0 & -t_r & 0 & l_r & 0 \\ 0 & 0 & 0 & 0 & 0 & 0 & 0 & 0 & 0 & 0 & 0 & 1 & 0 & 0 \\ 0 & 0 & 0 & 0 & 0 & 0 & 0 & 0 & 0 & 0 & 0 & 0 & 0 & 1 \\ 0 & 0 & 0 & 0 & 0 & 0 & 0 & 0 & 1 & 0 & 0 & 0 & 0 & 0 \end{bmatrix} \tag{24}$$

The kinetic observer model used to estimate the road profile in Step 2, is presented from Equations (25) to (30). The state vector (Equation (31)) contains the four wheel hop displacements and velocities and the road profile input. The control vector (Equation (26))

contains four suspension strut forces that are estimated based on the displacement measurements and suspension velocity estimations. The measurement vector (Equation (29)) consists of the estimated unsprung mass displacements and velocities determined with Step 1 of the algorithm.

Where

$$\boldsymbol{x}_k = \left\langle \begin{array}{cccccccccccc} z_1 & \dot{z}_1 & z_{01} & z_2 & \dot{z}_2 & z_{02} & z_3 & \dot{z}_3 & z_{03} & z_4 & \dot{z}_4 & z_{04} \end{array} \right\rangle^T \tag{25}$$

And

$$\boldsymbol{u}_k = \begin{array}{cccc} F_{FL} & F_{FR} & F_{RL} & F_{RR} \end{array}^T \tag{26}$$

And

$$\boldsymbol{F} = \begin{bmatrix} 1 & \Delta t & 0 & 0 & 0 & 0 & 0 & 0 & 0 & 0 & 0 & 0 \\ \frac{-\Delta t k_t}{m_1} & 1 & \frac{\Delta t k_t}{m_1} & 0 & 0 & 0 & 0 & 0 & 0 & 0 & 0 & 0 \\ 0 & 0 & 1 & 0 & 0 & 0 & 0 & 0 & 0 & 0 & 0 & 0 \\ 0 & 0 & 0 & 1 & \Delta t & 0 & 0 & 0 & 0 & 0 & 0 & 0 \\ 0 & 0 & 0 & \frac{-\Delta t k_t}{m_2} & 1 & \frac{\Delta t k_t}{m_2} & 0 & 0 & 0 & 0 & 0 & 0 \\ 0 & 0 & 0 & 0 & 0 & 1 & 0 & 0 & 0 & 0 & 0 & 0 \\ 0 & 0 & 0 & 0 & 0 & 0 & 1 & \Delta t & 0 & 0 & 0 & 0 \\ 0 & 0 & 0 & 0 & 0 & 0 & \frac{-\Delta t k_t}{m_3} & 1 & \frac{\Delta t k_t}{m_3} & 0 & 0 & 0 \\ 0 & 0 & 0 & 0 & 0 & 0 & 0 & 0 & 1 & 0 & 0 & 0 \\ 0 & 0 & 0 & 0 & 0 & 0 & 0 & 0 & 0 & 1 & \Delta t & 0 \\ 0 & 0 & 0 & 0 & 0 & 0 & 0 & 0 & 0 & \frac{-\Delta t k_t}{m_4} & 1 & \frac{\Delta t k_t}{m_4} \\ 0 & 0 & 0 & 0 & 0 & 0 & 0 & 0 & 0 & 0 & 0 & 1 \end{bmatrix} \tag{27}$$

And

$$\boldsymbol{B} = \begin{bmatrix} 0 & 0 & 0 & 0 \\ \frac{-\Delta t}{m_1} & 0 & 0 & 0 \\ 0 & 0 & 0 & 0 \\ 0 & 0 & 0 & 0 \\ 0 & \frac{-\Delta t}{m_2} & 0 & 0 \\ 0 & 0 & 0 & 0 \\ 0 & 0 & 0 & 0 \\ 0 & 0 & \frac{-\Delta t}{m_3} & 0 \\ 0 & 0 & 0 & 0 \\ 0 & 0 & 0 & 0 \\ 0 & 0 & 0 & \frac{-\Delta t}{m_4} \\ 0 & 0 & 0 & 0 \end{bmatrix} \tag{28}$$

Where

$$\boldsymbol{z}_k = \left\langle \begin{array}{cccccccc} \hat{z}_1 & \dot{\hat{z}}_1 & \hat{z}_2 & \dot{\hat{z}}_2 & \hat{z}_3 & \dot{\hat{z}}_3 & \hat{z}_4 & \dot{\hat{z}}_4 \end{array} \right\rangle^T \tag{29}$$

And

$$\boldsymbol{H} = \begin{bmatrix} 1 & 0 & 0 & 0 & 0 & 0 & 0 & 0 & 0 & 0 & 0 & 0 \\ 0 & 1 & 0 & 0 & 0 & 0 & 0 & 0 & 0 & 0 & 0 & 0 \\ 0 & 0 & 0 & 1 & 0 & 0 & 0 & 0 & 0 & 0 & 0 & 0 \\ 0 & 0 & 0 & 0 & 1 & 0 & 0 & 0 & 0 & 0 & 0 & 0 \\ 0 & 0 & 0 & 0 & 0 & 0 & 1 & 0 & 0 & 0 & 0 & 0 \\ 0 & 0 & 0 & 0 & 0 & 0 & 0 & 1 & 0 & 0 & 0 & 0 \\ 0 & 0 & 0 & 0 & 0 & 0 & 0 & 0 & 0 & 1 & 0 & 0 \\ 0 & 0 & 0 & 0 & 0 & 0 & 0 & 0 & 0 & 0 & 1 & 0 \end{bmatrix} \tag{30}$$

The prediction model used to predict the suspension forces in Step 3 uses a seven DOF model, complete with nonlinear suspension effects as modelled by Van der Westhuizen and Els [32]. The predictor model neglects tyre damping and assumes that the tyre may be modelled as a linear single point contact model that does not lose contact with the road. The predictor model is given in Equations (31) to (34).

Where

$$\boldsymbol{x} = \left\langle \begin{array}{cccccccccccccc} z_1 & \dot{z}_1 & z_2 & \dot{z}_2 & z_3 & \dot{z}_3 & z_4 & \dot{z}_4 & z_5 & \dot{z}_5 & \theta_x & \dot{\theta}_x & \theta_y & \dot{\theta}_y \end{array} \right\rangle^T \tag{31}$$

$$\boldsymbol{u} = \left\langle \begin{array}{cccccccc} \hat{F}_{FL} & \hat{F}_{FR} & \hat{F}_{RL} & \hat{F}_{RR} & \hat{z}_{01} & \hat{z}_{02} & \hat{z}_{03} & \hat{z}_{03} & g \end{array} \right\rangle^T \tag{32}$$

And

$$\boldsymbol{A} = \begin{bmatrix} 0 & 1 & 0 & 0 & 0 & 0 & 0 & 0 & 0 & 0 & 0 & 0 & 0 & 0 \\ \frac{-k_t}{m_1} & 0 & 0 & 0 & 0 & 0 & 0 & 0 & 0 & 0 & 0 & 0 & 0 & 0 \\ 0 & 0 & 0 & 1 & 0 & 0 & 0 & 0 & 0 & 0 & 0 & 0 & 0 & 0 \\ 0 & 0 & \frac{-k_t}{m_2} & 0 & 0 & 0 & 0 & 0 & 0 & 0 & 0 & 0 & 0 & 0 \\ 0 & 0 & 0 & 0 & 0 & 1 & 0 & 0 & 0 & 0 & 0 & 0 & 0 & 0 \\ 0 & 0 & 0 & 0 & \frac{-k_t}{m_3} & 0 & 0 & 0 & 0 & 0 & 0 & 0 & 0 & 0 \\ 0 & 0 & 0 & 0 & 0 & 0 & 0 & 1 & 0 & 0 & 0 & 0 & 0 & 0 \\ 0 & 0 & 0 & 0 & 0 & 0 & \frac{-k_t}{m_4} & 0 & 0 & 0 & 0 & 0 & 0 & 0 \\ 0 & 0 & 0 & 0 & 0 & 0 & 0 & 0 & 0 & 1 & 0 & 0 & 0 & 0 \\ 0 & 0 & 0 & 0 & 0 & 0 & 0 & 0 & 0 & 0 & 0 & 0 & 0 & 0 \\ 0 & 0 & 0 & 0 & 0 & 0 & 0 & 0 & 0 & 0 & 1 & 0 & 0 & 0 \\ 0 & 0 & 0 & 0 & 0 & 0 & 0 & 0 & 0 & 0 & 0 & 0 & 0 & 0 \\ 0 & 0 & 0 & 0 & 0 & 0 & 0 & 0 & 0 & 0 & 0 & 0 & 0 & 1 \\ 0 & 0 & 0 & 0 & 0 & 0 & 0 & 0 & 0 & 0 & 0 & 0 & 0 & 0 \end{bmatrix} \tag{33}$$

And

$$\boldsymbol{B} = \begin{bmatrix} 0 & 0 & 0 & 0 & 0 & 0 & 0 & 0 & 0 \\ \frac{-1}{m_1} & 0 & 0 & 0 & \frac{k_t}{m_1} & 0 & 0 & 0 & -1 \\ 0 & 0 & 0 & 0 & 0 & 0 & 0 & 0 & 0 \\ 0 & \frac{-1}{m_2} & 0 & 0 & 0 & \frac{k_t}{m_2} & 0 & 0 & -1 \\ 0 & 0 & 0 & 0 & 0 & 0 & 0 & 0 & 0 \\ 0 & 0 & \frac{-1}{m_3} & 0 & 0 & 0 & \frac{k_t}{m_3} & 0 & -1 \\ 0 & 0 & 0 & 0 & 0 & 0 & 0 & 0 & 0 \\ 0 & 0 & 0 & \frac{-1}{m_4} & 0 & 0 & 0 & \frac{k_t}{m_4} & -1 \\ 0 & 0 & 0 & 0 & 0 & 0 & 0 & 0 & 0 \\ \frac{1}{m} & \frac{1}{m} & \frac{1}{m} & \frac{1}{m} & 0 & 0 & 0 & 0 & -1 \\ 0 & 0 & 0 & 0 & 0 & 0 & 0 & 0 & 0 \\ \frac{t_l}{I_x} & \frac{-t_r}{I_x} & \frac{t_l}{I_x} & \frac{-t_r}{I_x} & 0 & 0 & 0 & 0 & 0 \\ 0 & 0 & 0 & 0 & 0 & 0 & 0 & 0 & 0 \\ \frac{-l_f}{I_y} & \frac{-l_f}{I_y} & \frac{l_r}{I_y} & \frac{l_r}{I_y} & 0 & 0 & 0 & 0 & 0 \end{bmatrix} \tag{34}$$

3.2. Prediction results

The vehicle model is first simulated driving on a Belgian paving in Adams [29] with the $4S_4$ suspension in the 'Ride Comfort' mode. The Belgian paving is part of the Suspension Track at Gerotek Test Facilities [36] and was measured experimentally by Becker and Els [9]. This road profile was implemented as a 3D regular grid road (RGR) model in Adams [29]. The simulated states are given as inputs to the suspension force prediction algorithm. The 'Ride Comfort' mode simulation is used to predict what the suspension strut force would be if the suspension mode was changed to 'Handling' mode.

Figure 8 shows the prediction results if the 'Ride Comfort' simulation is used to predict the suspension strut forces in that same suspension mode. Figure 9 shows the 'Handling' mode prediction results, based on the 'Ride Comfort' mode simulation.

Figures 8 and 9 show that the prediction algorithm can predict the suspension forces quite accurately, although the results are not as good as that of the linear quarter car results in Section 2. This is due to the fact that a seven DOF model is used to predict the forces simulated by a very complex vehicle model. The frequency content of the predicted forces is the most important aspect pertaining to the vehicle dynamics, a scaled, single-sized magnitude of the Fourier Transform of the front left suspension was included in Figures 8 and 9. Figure 8f shows that the frequency content of predicted suspension force in the 'Ride Comfort' suspension mode clearly indicates the peaks that are present in the simulated suspension forces. Figure 9f shows that the predicted suspension force in the 'Handling' mode (based on the measurements in the ride comfort mode) fails to capture the peak at 2 Hz, but that the peak at 4 Hz is captured accurately. This may be due to the suspension that is set to the 'Ride Comfort' mode attenuates low frequency content that is present due

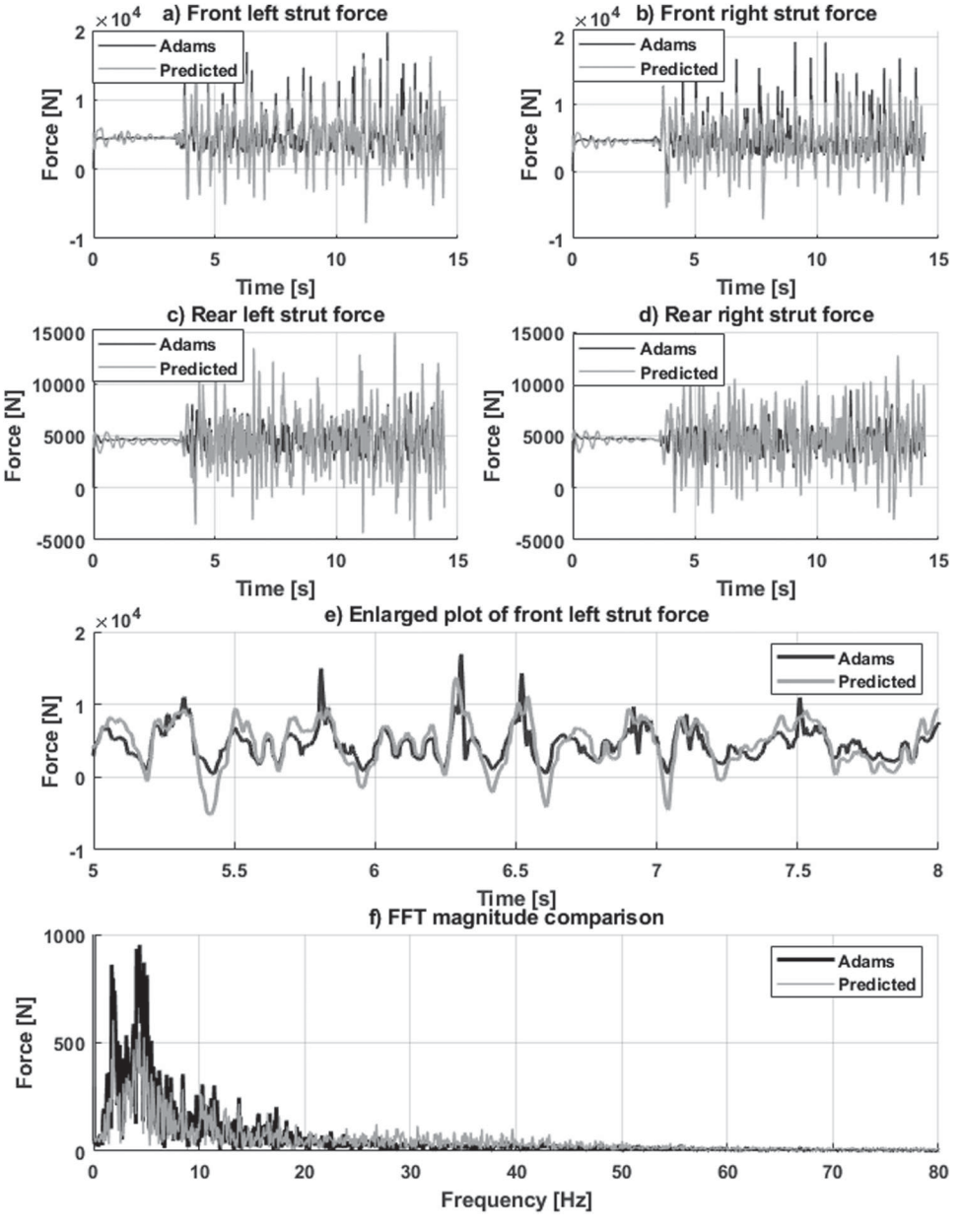

Figure 8. Suspension force prediction with 'Ride Comfort' suspension mode.

to the road profile content. The predicted force in the 'Handling' suspension mode (based on the 'Ride Comfort' mode measurements) thus underestimates the frequency content at very low frequencies.

One of the main contributing factors to the deterioration in performance may be the way that the tyre model is implemented in Step 3 of the prediction algorithm. Assuming

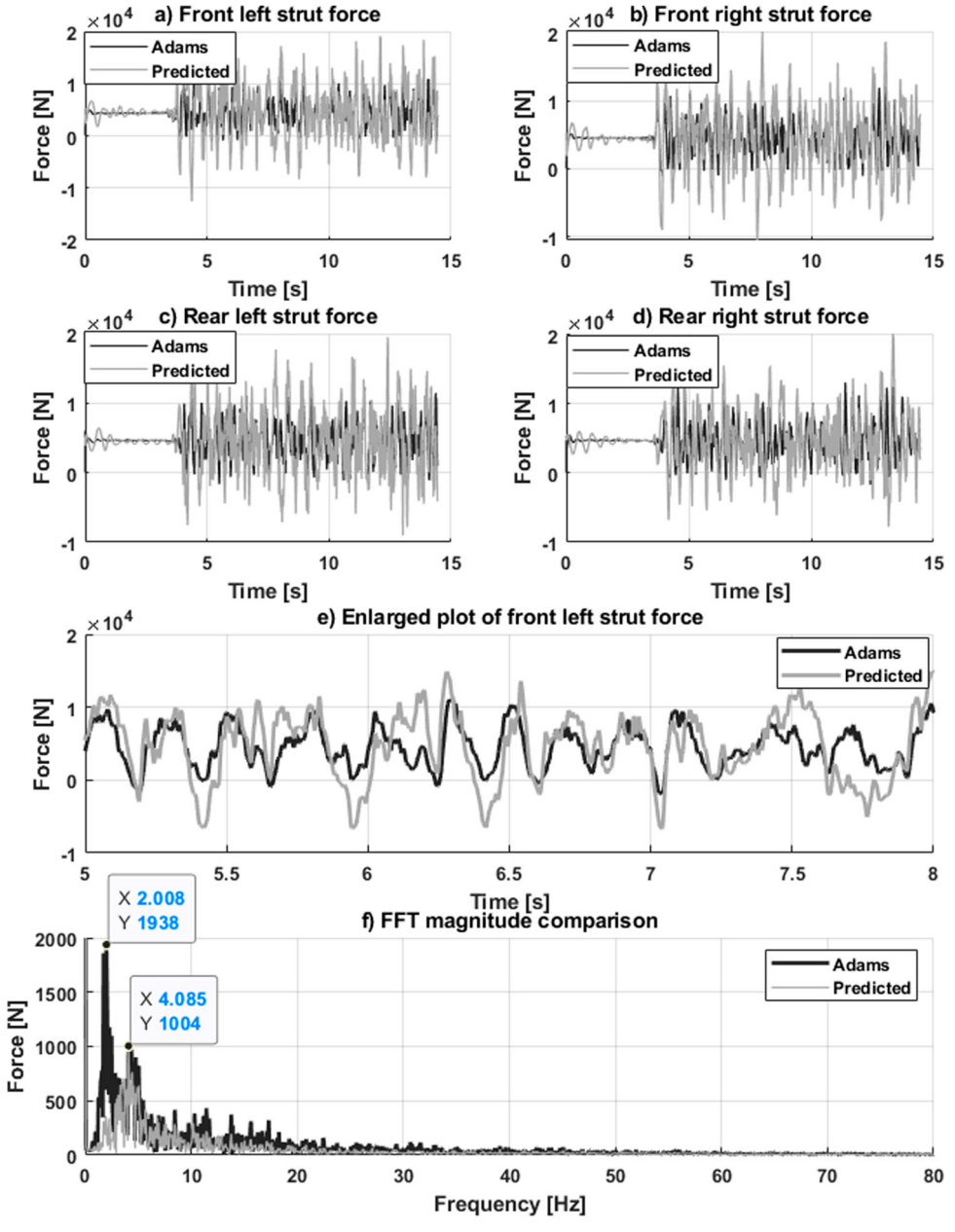

Figure 9. Prediction of suspension forces in 'Handling' suspension mode.

that the tyre may be modelled as a linear spring with no damping and that the tyre contact may be modelled as a single point contact that does not lose contact with the road is not really representative of the true tyre response and tyre-road interface. Including these effects will require the use of a more complex tyre model that can be used on rough roads with short wavelength irregularities. This tyre model will also need to run online, as the aim of the prediction algorithm is to provide information to the control system that chooses

Table 2. Sensors on instrumentedtest vehicle and their expected noise levels.

State	Symbol	Sensor	Sensor noise	Location	Algorithm section
Front leftunsprung mass acceleration	$\ddot{z}_1$	MEMSIC tri-axial accelerometer	25 mg	Front left upright	Kinematic observer controlvector (Equation (24))
Front right unsprung mass acceleration	$\ddot{z}_2$		25 mg	Front right upright	Kinematic observer controlvector (Equation (24))
Rear left unsprung mass acceleration	$\ddot{z}_3$		25 mg	Rear left upright	Kinematic observer controlvector (Equation (24))
Rear right unsprung mass acceleration	$\ddot{z}_4$		25 mg	Rear right upright	Kinematic observercontrol vector (Equation (24))
Sprung mass vertical acceleration	$\ddot{z}_5$	VBOXIntertial Measurement Unit (IMU)	150 μg	Sprung mass X-YCG	Kinematic observer control vector (Equation (24))
Sprung mass roll rate	$\dot{\theta}_x$		0.015°/s	Sprung mass X-YCG	Kinematic observer measurement vector (Equation (28))
Sprung mass pitch rate	$\dot{\theta}_y$		0.015°/s	Sprung mass X-YCG	Kinematic observer measurement vector (Equation (28))
Front leftsuspension displacement	x_{FL}	Celesco SP1 string potentiometer	0.25%	Front leftstrut	Kinematic observer measurement vector (Equation (28))
Frontright suspension displacement	x_{FR}		0.25%	Front right strut	Kinematic observer measurement vector (Equation (28))
Rear left suspension displacement	x_{RL}		0.25%	Rear left strut	Kinematic observer measurement vector (Equation (28))
Rear right suspension displacement	x_{RR}		0.25%	Rear right strut	Kinematic observer measurement vector (Equation (28))
Front leftstrut pressure	P_{FL}	WikaHigh-qualityS10pressure transducer	2bar	Front leftstrut	Algorithm validation
Frontright strut pressure	P_{FR}		2bar	Front right strut	Algorithm validation
Rear left strut pressure	P_{RL}		2bar	Rear left strut	Algorithm validation
Rear right strut pressure	P_{RR}		1.25bar	Rear right strut	Algorithm validation
Vehicle speed	v	VBOX 3i RTK dual antenna GPS	0.03 km/h	Vehicle roof	General information

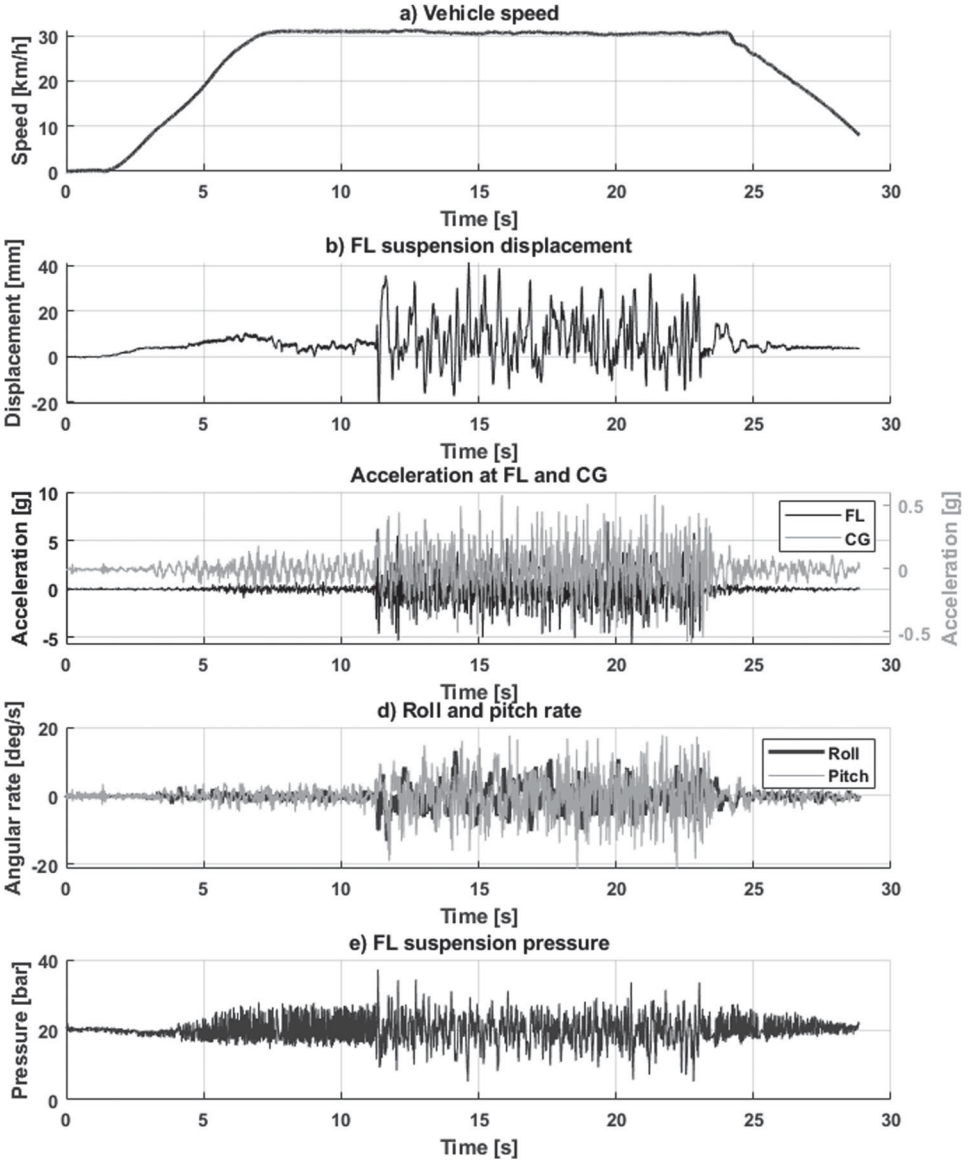

Figure 10. Sensor time histories on Belgian paving in 'Ride Comfort' suspension mode (limited to FL suspension strut for clarity).

the suspension mode. Recently, cosin [37] has developed a real-time version of FTire that may be used in the future [38]. All of these factors may contribute to the overestimation of higher frequency content and underestimation of lower frequency content in the predicted suspension forces.

4. Experimental results

The final step in validating the suspension force prediction algorithm is to implement it on the test vehicle. The test vehicle (the Land Rover Defender discussed in Section 3) was

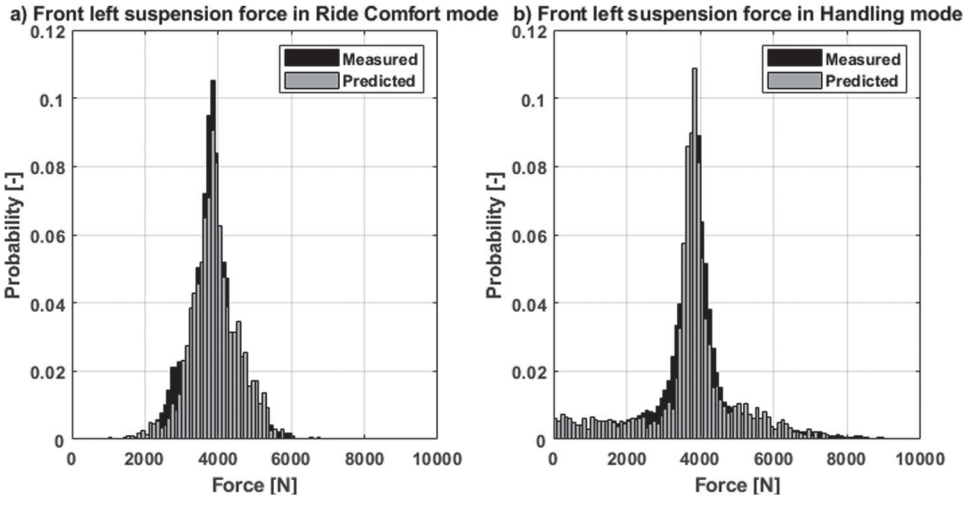

Figure 11. Front left suspension strut force with (a) 'Ride Comfort' mode prediction and (b) 'Handling' mode prediction.

instrumented with the equipment listed in Table 2. The sensor noise indicated in Table 2 influenced the tuning of the covariance matrices included in Appendix A. Data was recorded on a dSPACE MicroAutoBox II, a robust and compact stand-alone real-time system that combines high performance with comprehensive I/O [39]. Data was sampled at 1000 Hz.

Tests were conducted on the Belgian paving at Gerotek Test Facilities [36]. The test vehicle was driven at a constant speed across the Belgian paving while recording the time histories of the sensors listed in Table 2. Test runs were conducted in 'Ride Comfort' and 'Handling' suspension modes. Figure 10 shows an example of the measured data during a test run in 'Ride Comfort' mode on the Belgian paving.

The recorded data of the 'Ride Comfort' mode test runs were given as input to the suspension force prediction algorithm. The predicted suspension forces were then compared with suspension forces measured during 'Handling' mode runs. Because the predicted 'Handling' mode suspension force is based on 'Ride Comfort' mode test runs, it is difficult to compare the prediction in the time domain. Normalised histograms of the suspension forces (both the predicted force and the force derived from the suspension strut pressure measurements) are used to visually compare the prediction results. The results of the front left suspension force prediction on the Belgian paving at 30 km/h are shown in Figure 11. Figure 12 shows the 'Handling' mode prediction results for all four suspension struts on the Belgian paving based on data recorded during a 'Ride Comfort' test run.

The results shown in Figures 11 and 12 indicate that the suspension force prediction algorithm is capable of predicting the suspension force before switching the suspension from one mode to another. There are some discrepancies between the measured and predicted forces. These discrepancies are due to:

(1) During testing, it is impossible to drive exactly the same path at the same speed in successive test runs. These differences in speed and position may influence the suspension

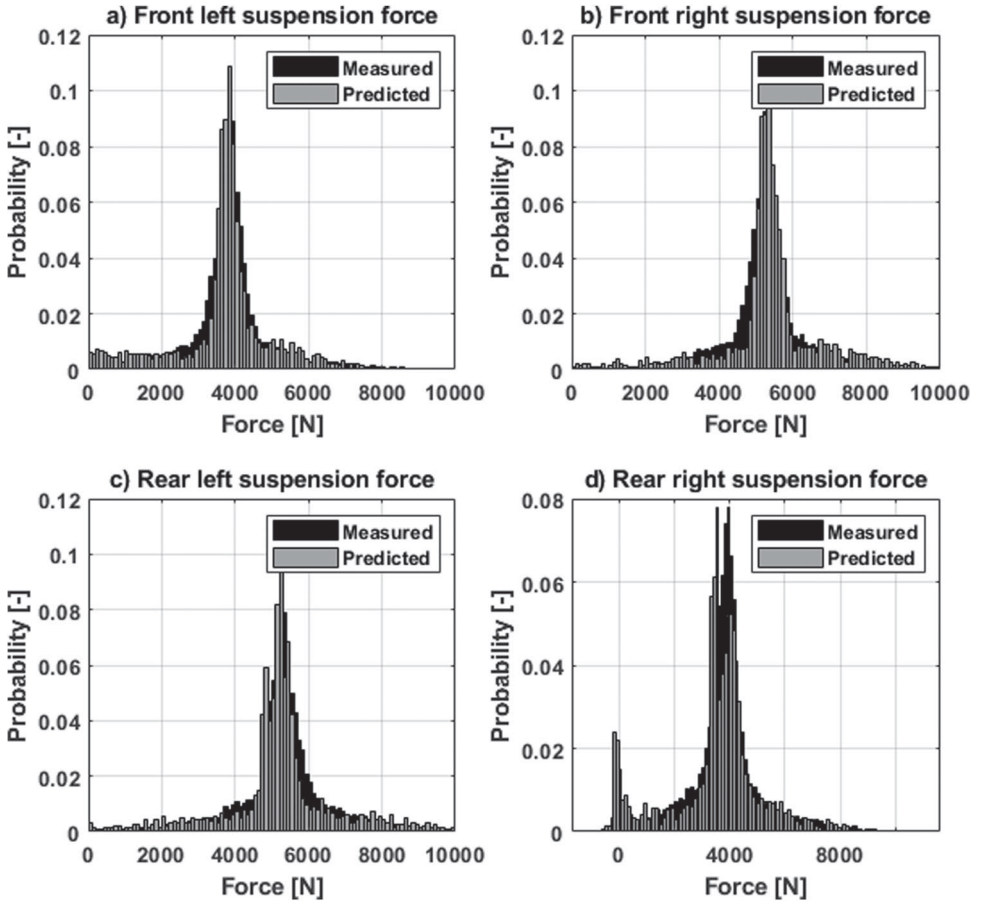

Figure 12. 'Handling' mode prediction results for all four struts on Belgian paving with 'Ride Comfort' measurements.

forces when comparing measurements and predictions from two separate test runs.

(2) The prediction model relies on accurate models of the suspension force characteristics. While all practicable measures were taken to ensure that the suspension model used is accurate (such as ensuring that the gas mass charged into the accumulators is correct), small inaccuracies may accumulate in large errors. This was confirmed by Van der Westhuizen and Els [32], especially for the case of the 'Handling' suspension mode. In the 'Handling' suspension mode, the gas volume is very small. Even the slightest error when charging gas to the accumulator may have a significant effect.

(3) The estimation and prediction models neglect suspension kinematics, tyre non-linearity and tyre damping. The tyre-road interface is also simplified significantly.

During analysis of the data, it was also noticed that the quality of the sensor measurements significantly influences the performance of the algorithm and care should be taken when instrumenting and maintaining a vehicle with sensors such as these.

Despite these discrepancies, the performance of the algorithm on the Belgian paving is seen to be similar to that reported in Sections 2 and 3.

5. Conclusion and future work

The aim of this paper was to develop a suspension force prediction algorithm that can predict the suspension force before a control decision is made. The developed algorithm uses three stages, namely (1) estimating the sprung and unsprung mass motions with a kinematic KF, (2) estimating the road excitation with a kinetic KF and (3) predicting the suspension force with a predictor model. The algorithm's performance was evaluated in simulation first, using a linear quarter car and then a full vehicle model in Adams for comparing. Finally the algorithm's performance was evaluated against experimental results.

It is concluded that the algorithm successfully predicted the suspension forces in 'Handling' mode while the suspension was set to 'Ride Comfort' mode.

Future work and further investigations and fine tuning of the prediction algorithm include:

(1) Conducting a sensitivity analysis to see how the algorithm performs on different road surfaces and at different speeds.
(2) The current investigation focussed mainly on predicting suspension forces on undulating roads where comfort is the default suspension setting in all likelihood. The investigation may be extended to other manoeuvres such as a double lane change where the suspension is probably in a handling mode. In the event that the vehicle then leaves the road (due to the avoidance manoeuvre), it may be beneficial to revert back to a comfort suspension setting.
(3) Currently, the algorithm is driven by road input. Possible expansion to changes in suspension force due to driver input may further enhance its capability.
(4) At the moment, the suspension force prediction was only evaluated while the vehicle was driving at a constant speed. The performance should also be evaluated while the vehicle is accelerating or decelerating, as would be the case when performing an emergency stop.
(5) Quantifying the performance using an objective metric.
(6) Further investigating and evaluating the value of the estimated road profile and its relation to the actual road profile.

Nomenclature

Symbol	Description	Unit	Symbol	Description	Unit
$\boldsymbol{B}$	Control matrix	[—]	$\boldsymbol{R}$	Observation noise covariance matrix	[—]
CG	Centre of gravity	[—]	$\boldsymbol{Q}$	Process noise covariance matrix	[—]

c	Damping coefficient	[N.s/m]	RL	Rear left	[—]
c_t	Tyre vertical damping	[N.s/m]	RMS	Root mean square	[—]
DGPS	Differential global positioning system	[—]	RR	Rear right	[—]
DOF	Degree of freedom	[—]	$\boldsymbol{S}$	Measurement residual covariance matrix	[—]
$\boldsymbol{F}$	State transition matrix	[—]	t	Time	[s]
F_i	Suspension strut force, where $i \in \{FL, FR, RL, RR\}$	[N]	t_l	Distance from left wheels to sprung mass CG	[m]
$\hat{F}_i$	Estimated suspension strut force, where $i \in \{FL, FR, RL, RR\}$	[N]	t_r	Distance from right wheels to sprung mass CG	[m]
$F(i\omega)$	Fourier series	[—]	$\boldsymbol{u_k}$	Control vector at time step k	[—]
FL	Front left	[—]	v	Vehicle speed	[m/s]
$f_{n,sm}$	Sprung mass natural frequency	[Hz]	$\boldsymbol{v}_k$	Observation noise at time step k	[—]
$f_{n,usm}$	Unsprung mass natural frequency	[Hz]	w	Exponent of fitted PSD calculated on G_d	[—]
FR	Front right	[—]	$\boldsymbol{w_k}$	Process noise at time step k	[—]
$G_d(.)$	Vertical displacement PSD of road profile	[m^3]	x_i	Suspension strut relative displacement, where $i \in \{FL, FR, RL, RR\}$	[m]
g	Gravitational acceleration	[m/s^2]	$\boldsymbol{x}_k$	State vector at time step k	[—]
$\boldsymbol{H}$	Observation model	[—]	$\hat{\boldsymbol{x}}$	State vector estimate	[—]
$\boldsymbol{I}$	Identity matrix	[—]	$\boldsymbol{z}_k$	Observation vector at time step k	[—]
IMU	Inertial measurement unit		$\tilde{\boldsymbol{z}}_{\boldsymbol{k}}$	Measurement residual at time step k	[—]
I/O	Input / Output	[—]	z_0	Road profile input	[m]
I_x	Sprung mass roll inertia	[kg.m^2]	z_i	Road profile input, where $i \in \{01, 02, 03, 04\}$	[m]
I_y	Sprung mass pitch inertia	[kg.m^2]	$\hat{z}_i$	Estimated road profile input, where $i \in \{01, 02, 03, 04\}$	[m]
$\boldsymbol{K}$	Optimal Kalman gain	[—]	z_1	Unsprung mass vertical displacement or front left unsprung mass vertical displacement, depending on context	[m]
k	Spring stiffness	[N/m]	z_2	Sprung mass vertical displacement or front right unsprung mass vertical displacement, depending on context	[m]
KF	Kalman filter		z_3	Rear left unsprung mass vertical displacement	[m]
k_t	Tyre vertical stiffness	[N/m]	z_4	Rear right unsprung mass vertical displacement	[m]
LVDT	Linear variable differential transformer	[—]	z_5	Sprung mass vertical displacement	[m]
l_f	Distance from front axle to sprung mass CG	[m]	$\dot{z}_i$	Time derivative of z_i, where $i \in \{1, 2, 3, 4, 5\}$	[m/s]
l_r	Distance from rear axle to sprung mass CG	[m]	$\ddot{z}_i$	Time derivative of $\dot{z}_i$, where $i \in \{1, 2, 3, 4, 5\}$	[m/s^2]
M	Sprung mass	[kg]			
m	Unsprung mass	[kg]	α	Fourier series phase angle	[rad]
m_i	Unsprung mass of i^{th} corner, where $i \in \{1, 2, 3, 4\}$	[kg]	θ_x	Sprung mass roll angle	[rad]
n	Spatial frequency	[cycles/m]	$\dot{\theta}_x$	Sprung mass roll rate	[rad/s]
n_0	Reference spatial frequency	[cycles/m]	θ_y	Sprung mass pitch angle	[rad]
$\boldsymbol{P}$	State estimate covariance matrix	[—]	$\dot{\theta}_y$	Sprung mass pitch rate	[rad/s]
P_i	Pressure in suspension strut, where $i \in \{FL, FR, RL, RR\}$	[Pa]			

Disclosure statement

No potential conflict of interest was reported by the author(s).

References

[1] Els PS, Botha T, Hamersma H, et al., editors. The effect of controllable suspension settings on the ABS braking performance of an off-road vehicle on rough terrain. Proceedings of the 7th ISTVS Regional Americas Conference at Tampa, Florida; 2013.

[2] Hamersma HA, Els PS. Improving the braking performance of a vehicle with ABS and a semi-active suspension system on a rough road. J Terramechanics. 2014 Dec;56:91–101.

[3] Els PS. The ride comfort vs. handling compromise for off-road vehicles [PhD dissertation]. Pretoria: University of Pretoria; 2006.

[4] Fischer D, Isermann R. Mechatronic semi-active and active vehicle suspensions. Control Eng Pract. 2004;12(11):1353–1367.

[5] Giliomee CL, Els PS. Semi-active hydropneumatic spring and damper system. J Terramechanics. 1998 Apr;35(2):109–117.

[6] Strydom A, Els PS, Kaul S. Magneto-Rheological (Mr) Damper modeling for semi-active control without force feedback. Proceedings of the Asme International Design Engineering Technical Conferences and Computers and Information in Engineering Conference 2012, Vol 1, Pts a and B. 2012:1145–1153.

[7] Gillespie TD. Fundamentals of vehicle dynamics. Warrendale (PA): SAE International; 1992.

[8] Imine H, Delanne Y, M'Sirdi NK. Road profile input estimation in vehicle dynamics simulation. Vehicle Syst Dyn. 2006;44(4):285–303.

[9] Becker CM, Els PS. Profiling of rough terrain. Int J Vehicle Des. 2014;64(2–4):240–261.

[10] Splanger E, Kelly W. Road profilometer method for measuring road profile. General Motors Research Publication GMR-452. 1964.

[11] Botha TR, Els PS. Rough terrain profiling using digital image correlation. J Terramechanics. 2015 Jun;59:1–17.

[12] International Organisation of Standardisation. ISO 8608:2016 Mechanical vibration – Road surface profiles – Reporting of measured data. Geneva, Switzerland.

[13] Agostinacchio M, Ciampa D, Olita S. The vibrations induced by surface irregularities in road pavements – a Matlab® approach. Eur Transp Res Rev. 2014 Sept;6(3):267–275.

[14] Imine H, M'sirdi N, Delanne Y. Adaptive observers and estimation of the road profile. SAE Technical Paper; 2003.

[15] Imine H, Fridman L. Road profile estimation in heavy vehicle dynamics simulation. Int J Vehicle Des. 2008;47(1/2/3/4):234–249.

[16] Imine H, Madani T. Heavy vehicle suspension parameters identification and estimation of vertical forces: experimental results. Int J Control. 2015;88(2):324–334.

[17] Doumiati M, Victorino A, Charara A, et al., editors. Estimation of road profile for vehicle dynamics motion: experimental validation. 2011 American Control Conference; 2011 June 29–July 1, 2011; San Francisco, CA, USA.

[18] Doumiati M, Martinez J, Sename O, et al. Road profile estimation using an adaptive Youla–Kučera parametric observer: comparison to real profilers. Control Eng Pract. 2017;61:270–278.

[19] Ben Hassen B, Miladi M, Abbes MS, et al. Road profile estimation using the dynamic responses of the full vehicle model. Appl Acoust. 2017;147(April 2019):87–99.

[20] Ray LR. Nonlinear state and tire force estimation for advanced vehicle control. IEEE Trans Control Syst Technol. 1995;3(1):117–124.

[21] Antonov S, Fehn A, Kugi A. Unscented Kalman filter for vehicle state estimation. Vehicle Syst Dyn. 2011;49(9):1497–1520.
[22] Pence BL, Fathy HK, Stein JL. Sprung mass estimation for off-road vehicles via base-excitation suspension dynamics and recursive least squares. 2009 American Control Conference; June 10–12, 2009; St Louis, MO, USE2009.
[23] Wenzel TA, Burnham KJ, Blundell MV, et al. Dual extended Kalman filter for vehicle state and parameter estimation. Vehicle Syst Dyn. 2006;44(2):153–171.
[24] Vazquez AGA, Vaseur C, Correa-Victorino A, et al. Road profile and suspension state estimation boosted with vehicle dynamics conjectures. 2019 IEEE Intelligent Vehicles Symposium (IV); 2019 9–12 June 2019.
[25] Kalman RE. A new approach to linear filtering and prediction problems. J Basic Eng. 1960;82(1):35–45.
[26] MathWorks. MATLAB and Simulink 2016 [20 July 2016]. Available from: http://www.mathworks.com/
[27] Stallmann MJ, Els PS. Parameterization and modelling of large off-road tyres for ride analyses: part 2 – parameterization and validation of tyre models. J Terramechanics. 2014 Oct;55:85–94.
[28] Kat CJ, Els PS. Validation metric based on relative error. Math Comp Model Dyn. 2012;18(5):487–520.
[29] MSC Software. Adams: MSC Software Corporation; 2016 [18 July 2016]. Available from: http://www.mscsoftware.com/product/adams
[30] Thoresson MJ, Uys PE, Els PS, et al. Efficient optimisation of a vehicle suspension system, using a gradient-based approximation method, Part 1: mathematical modelling. Math Comput Model. 2009 Nov;50(9–10):1421–1436.
[31] Uys P, Els P, Thoresson M, et al. Experimental determination of moments of inertia for an off-road vehicle in a regular engineering laboratory. Int J Mech Eng Educ. 2006;34(4):291–314.
[32] Van der Westhuizen SF, Els PS. Comparison of different gas models to calculate the spring force of a hydropneumatic suspension. J Terramechanics. 2015 Feb;57:41–59.
[33] Theron NJ, Els PS. Modelling of a semi-active hydropneumatic spring damper unit. Int J Vehicle Des. 2007;45(4):501–521.
[34] Gipser M. FTire – the tire simulation model for all applications related to vehicle dynamics. Vehicle Syst Dyn. 2007;45(Supp1):139–151.
[35] Bosch H-RB, Hamersma HA, Els PS. Parameterisation, validation and implementation of an all-terrain SUV FTire tyre model. J Terramechanics. 2016;67:11–23.
[36] Armscor Defence Institutes SOC. Gerotek Test Facilities [12 July 2016]. Available from: http://www.armscordi.com/SubSites/Gerotek1/Gerotek01_landing.asp
[37] Cosin Scientific Software. Cosin scientific software 2018 [22 March 2018]. Available from: https://www.cosin.eu/
[38] dSPACE GmbH. FTire and ASM - Sophisticated Models for Real-Time Vehicle Dynamics Simulation 2016 [22 March 2018]. Available from: https://www.cosin.eu/wp-content/uploads/FTire_Artikel_VehicleDynamic_1601213.pdf
[39] dSPACE GmbH. MicroAutoBox II 2017 [16 October 2018]. Available from: https://www.dspace.com/shared/data/pdf/2017/dSPACE_MicroAutoBoxII_Brochure_2017-A_170703_E.pdf

Appendix A. Kalman filter noise covariance matrices

Linear quarter car implementation

Step 1: Estimating the sprung mass and unsprung mass displacement

$$\boldsymbol{Q}_k = \text{diag}(0.5 \quad 0.5)$$

$$\boldsymbol{R}_k = \text{diag}\begin{pmatrix}1 & 1e6\end{pmatrix}$$

Step 2: Estimating the road excitation

$$\boldsymbol{Q}_k = \text{diag}\begin{pmatrix}0.01 & 0.1 & 100\end{pmatrix}$$
$$\boldsymbol{R}_k = \text{diag}\begin{pmatrix}0.01 & 0.1\end{pmatrix}$$

Full vehicle model implementation

Step 1: Estimating the sprung mass and unsprung mass displacement

$$\boldsymbol{Q}_k = \boldsymbol{I}^{[14\times14]}$$
$$\boldsymbol{R}_k = \text{diag}\begin{pmatrix}0.1 & 0.1 & 0.1 & 0.1 & 1 & 1 & 1 & 1 & 1 & 1 & 100\end{pmatrix}$$

Step 2: Estimating the road excitation

$$\boldsymbol{Q}_k = \boldsymbol{I}^{[12\times12]}$$
$$\boldsymbol{R}_k = \text{diag}\begin{pmatrix}1 & 1 & 1 & 1 & 1 & 1 & 1 & 1 & 100 & 100 & 100 & 100\end{pmatrix}$$

Physical implementation on experimental vehicle

Step 1: Estimating the sprung mass and unsprung mass displacement

$$\boldsymbol{Q}_k = \text{diag}\begin{pmatrix}10 & 1e4 & 1 & 1e4 & 1 & 1e4 & 1 & 1e4 & 1 & 1e3 & 10 & 100 & 10 & 100\end{pmatrix}$$
$$\boldsymbol{R}_k = \text{diag}\begin{pmatrix}0.5 & 0.5 & 0.5 & 0.5 & 1 & 1 & 1e6 & 1e6 & 1e6 & 1e6 & 1e6\end{pmatrix}$$

Step 2: Estimating the road excitation

$$\boldsymbol{Q}_k = \boldsymbol{I}^{[12\times12]}$$
$$\boldsymbol{R}_k = \boldsymbol{I}^{[8\times8]}$$